Chemical Engineering Journal 360 (2019) 1199–1212

Contents lists available at ScienceDirect

Chemical Engineering Journal

journal homepage: www.elsevier.com/locate/cej

Nitrogen-rich hierarchically porous polyaniline-based adsorbents for carbon dioxide (CO_2) capture

Edith Mawunya Kutorglo[a,*], Fatima Hassouna[a], Anna Beltzung[b], Dušan Kopecký[c], Ivona Sedlářová[d], Miroslav Šoóš[a,*]

[a] Department of Chemical Engineering, University of Chemistry and Technology, Technická 3, 166 28 Prague 6 – Dejvice, Czech Republic
[b] Institute for Chemistry and Bioengineering, Department of Chemistry and Applied Biosciences, ETH Zurich, Vladimir-Prelog-Weg 1-5/10, 8093 Zürich, Switzerland
[c] Department of Physics and Measurements, University of Chemistry and Technology, Technická 3, 166 28 Prague 6 – Dejvice, Czech Republic
[d] Department of Inorganic Technology, University of Chemistry and Technology, Technická 5, 166 28 Prague 6 – Dejvice, Czech Republic

HIGHLIGHTS

- Hierarchically porous materials were synthesized using an easy and new concept.
- The materials were prepared from cheap precursors and applied in CO_2 capture.
- The pore size distribution was easily tuned by changing the size of nanoparticles.
- The high CO_2 sorption capacity is among the highest reported for carbon materials.
- The approach provides a strategy serving as a guide to the design of new CO_2 capture sorbents.

GRAPHICAL ABSTRACT

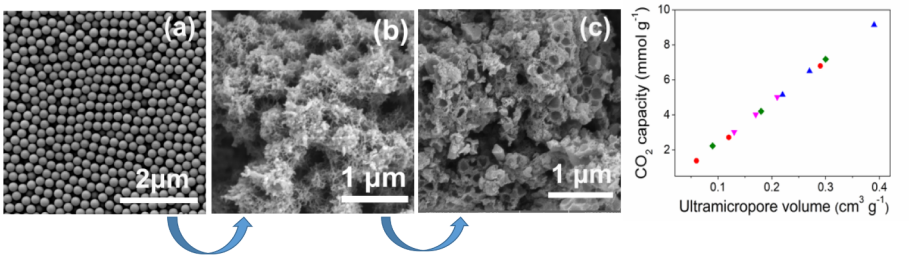

ARTICLE INFO

Keywords:
Hierarchical pore structure
Carbon dioxide capture
Nitrogen rich
Polyaniline
Adsorption
Porous materials

ABSTRACT

The development of new materials and technologies for CO_2 capture has attracted a lot of interest due to the growing concerns about global warming and climate change. Herein, we prepared hierarchically porous materials from cheap precursors – polyaniline and polystyrene nanoparticles (PS NPs) using an easy and new concept based on the removal of the PS NPs during a pre-carbonization step followed by chemical activation. The pore size distribution was easily tuned by varying the size of the sacrificial PS NPs and the intensity of chemical treatment. We obtained an outstanding CO_2 capture capacity of our optimum material (9.14 mmol g^{-1} at 273.15 K and 1 bar). The findings suggest that these materials are promising CO_2 sorbents and the approach provides a strategy to design new high-capacity polymer-based carbons for CO_2 capture.

1. Introduction

The heavy reliance on fossil fuels for energy has led to a drastic rise in atmospheric CO_2 emissions. This has raised a lot of concerns given the steady increase in global temperatures, commonly known as global warming, of which anthropogenic CO_2 emissions have been directly implicated [1–3]. Carbon capture and storage (CCS) from large emission sources is considered as immediate and most realistic solution to minimize CO_2 emissions while searching for long-term sustainable energy sources to replace fossil fuels [4,5]. Among the CO_2 capture

* Corresponding authors.
E-mail addresses: kutorgle@vscht.cz (E.M. Kutorglo), soosm@vscht.cz (M. Šoóš).

https://doi.org/10.1016/j.cej.2018.10.133
Received 20 July 2018; Received in revised form 21 September 2018; Accepted 13 October 2018
Available online 17 October 2018

options available, post-combustion capture is the most widely adopted method, thanks to its flexibility and the fact that it can be easily retrofitted to already existing fossil fuel power plants [1,6]. For more than 60 years, aqueous amine absorption has been an efficient technology for the removal of CO_2 from natural gas. However, this technique has several drawbacks, such as corrosion of equipment and high amounts of energy are needed for regeneration of the solvents making the process expensive [2,5,7]. The main challenge for realizing practical carbon capture lies with the design of new sorbents from cheap materials, with high capacity and easy recyclability.

Over the past few decades, a number of solid sorbents e.g. molecular sieves, porous carbon, porous silica, metal organic frameworks etc., are emerging as good alternatives to replace liquid amines, given their well developed porosity, easy handling and lower energy requirements for regeneration [7–9]. Based on the materials studied so far, it has been found that efficient CO_2 sorption performance depends on a combination of diffusion and adsorption selectivity [10–12]. Therefore, a good CO_2 sorbent comprises high microporosity with suitable pore sizes (ultramicropores with diameters < 0.7 nm), coupled with the presence of bigger pores, to enhance efficient diffusion [13]. An additional parameter reported to influence CO_2 sorption is the presence of appropriate surface functionalities (nitrogen or other heteroatoms). Many different mechanisms have been proposed to explain the increase of CO_2 sorption on nitrogen-doped carbon materials such as Lewis acid-Lewis base interaction [14–16], quadrupolar interaction [17,18] and hydrogen bonding interaction [19]. Specifically, it was previously reported that the pyrrolic and amine nitrogen functionalities have the strongest interactions with CO_2 molecules [15,20,21].

Several authors have attempted to explain the differences in the mechanisms of CO_2 adsorption in micropores and in the presence of nitrogen functionalities. When a sorbent material is highly ultramicroporous, where their pore aperture is similar to the size of CO_2 molecules, adsorption occurs mainly by physisorption mechanisms such as capillary condensation and molecular sieving and the role of nitrogen functionalities becomes less obvious. When the materials are mesoporous, and therefore the capillary effect diminishes, it is then the chemisorption binding mechanisms dominate and nitrogen functionalities play the major role [7]. Additionally, because CO_2 is a weak Lewis acid, its adsorption capacity is influenced by the surface chemistry [6], suggesting that a synergistic contribution between the hierarchical porosity (micro- and mesopores) coupled with appropriate surface chemistry (nitrogen functionalities) is essential to achieve high sorption capacities. This may be the reason why it has been difficult to make a direct correlation between the simultaneous contribution of nitrogen and textural properties in the same material towards its CO_2 uptake capacity, especially if the material has a hierarchical pore structure with contributions from both micro- and mesopores.

From these findings, a lot of research has been focused on designing new sorbents using two main approaches: (i) post-synthetic functionalization to incorporate nitrogen or oxygen groups onto the porous framework and (ii) direct carbonization and activation of nitrogen-containing polymers [13,19,22]. The latter approach is more promising since it allows better control over the chemical composition and eliminates the usually complicated post-treatments to incorporate nitrogen or other functional groups [10,23], which usually results in the blockage of the diffusion channels to the active sites present on the materials [24,25]. Moreover, there have been reports of amine degradation and leaching after multiple CO_2 capture cycles leading to instability of these materials and limiting their long-term use [8,26,27]. Recently several N-bearing microporous carbon sorbents have been prepared from N-based precursors such as polyacrylonitrile [28], polyaniline [29], polypyrrole [22], and other renewable resources such as soya bean dregs [30] and saw dust [31] by various methods, mainly using KOH as activating agent. These materials have been shown to exhibit high sorption capacities and are promising for CO_2 capture applications. Specifically, Wickramarante et al. [32] successfully synthesized phenolic resin-based activated carbon spheres with the optimum material CS*-P-A exhibiting high surface area (S_{BET} = 2400 m^2/g) and a corresponding high CO_2 capacity of 8.9 mmol g^{-1} at 1 bar and 273 K. Similarly, Lee et al. [11] prepared polypyrrole-based porous materials and the materials exhibit high microporosity and high sorption capacities up to 7.30 mmol g^{-1} for their optimized material (600-2). Many of these experimental studies have been supported by molecular simulations on CO_2 adsorption behavior, which attribute high CO_2 capacities to high microporosity and the presence of surface functionalities (nitrogen, oxygen and sulfur) [13,33–35]. The incorporation of heteroatoms into carbon framework is thought to enhance uptake due to increased polarity of the carbon surface. However, tuning the diffusion and adsorption selectivity in these materials is not synergistic. Generally, the conditions required for generating high amount of small pores (high temperature and chemical treatment e.g. using KOH) results in the loss of surface functionalities [36–38]. For instance, Xing et al. [19] prepared a series of N-doped carbons from bean dreg by chemical activation and observed an inverse relationship between the nitrogen content and both the KOH amount and activation temperature. In a similar study, the content of sulfur in nanoporous carbon was found to decrease whereas the porosity increased upon air oxidation at 350 °C [39]. Moreover, it has been known that porous materials consisting solely of micropores suffer from diffusion problems, suggesting that the optimally designed sorbent should have a hierarchical pore structure. Therefore, it still remains a challenge to design the perfect combination of a material framework and surface chemistry. In other words, materials comprising all three types of pores i.e. abundant micropores (for high CO_2 adsorption), mesopores and macropores (to facilitate efficient CO_2 diffusion into and out of the adsorption sites) coupled with appropriate surface functionalities [40,41], will be the optimal sorbent.

In our earlier work, we reported the preparation of 3-D macroporous polyaniline (PANI) materials with very high porosities by a simple approach using polystyrene nanoparticles (PS NPs) as support blocks onto which PANI can easily adsorb and form 3-D networks [42]. To create a material comprising all three types of pores while preserving surface functional groups, we used a simple approach involving sacrificial PS NPs to prepare stable hierarchically porous materials with high surface areas and abundant surface groups and tested their application in CO_2 capture. Our strategy, which is based on an extension of our previous synthetic approach, involves the removal of sacrificial PS NPs during a pre-carbonization step followed by chemical activation using KOH. By changing the size of the PS NPs and KOH/C ratio for activation, it is possible to tune the pore size distribution and sorption capacity of the materials. The optimized material achieved very high CO_2 capacity (9.14 mmol g^{-1}) at 273.15 K and 1 bar, which is among the highest reported for carbon-based sorbents in the literature.

2. Materials and methods

2.1. Materials

Styrene (St, > 99%), ammonium peroxydisulfate (APS, 98%), poly (vinyl pyrrolidone) (PVP, Mw = 40000 g mol^{-1}), aniline (ANI, ACS reagent, > 99.5%), phytic acid solution 50% (w/w) in H_2O were all purchased from Sigma Aldrich and used without modification or purification.

2.2. Synthesis of monodisperse PS nanoparticles and the 3-D microclusters

The PS-NP building blocks were prepared by radical emulsion polymerization according to the procedure described in Kutorglo et al. [42]. The recipe for preparing 370 nm PS NPs is presented in Table 1(A) while that for the preparation of PANI and crosslinked PANI is shown in Table 1(B). Aniline (ANI) was polymerized by chemical oxidative route in aqueous medium at 4 °C in an ice water bath in the presence of the PS

Table 1
Recipe for the preparation of (A) monodisperse 370 nm PS NPs by emulsion polymerization and (B) PS-PANI aggregates.

Parameter	Composition
(A) PS-NPs	
Solid content	20 wt%
Ratio styrene/PVP	56.25 (-)
Ratio monomer/initiator	100 (-)
(B) PANI Microclusters	
Solid content	5 wt%
Ratio of PS NPs/aniline (ANI)	1 (-)
Ratio of initiator (APS)/ANI	2.5 (-)
Ratio of phytic acid/ANI	2 (-)
Concentration of APS solution	1.56 mol L^{-1}
Rate of addition of APS solution	0.5 mL min^{-1}

NPs. APS was used as initiator and HCl as dopant, which was also used to maintain the pH of the polymerization medium in acidic range. Additionally, polymerization of ANI was done without PS NPs, with or without phytic acid as crosslinker for comparison. In a typical synthesis, ANI was added to HCl solution (1 M) under stirring followed by addition of phytic acid. After stirring at 250 rpm using a magnetic stirrer for some time (approx. 15 min), PS NPs were added to the mixture and stirred for another 10 min. APS was then dissolved in HCl solution (1 M) and added to the ANI-PS mixture slowly using a syringe pump. The polymerization was allowed to run overnight for at least 16 h. The resulting suspension of microclusters was freeze dried to obtain dry product for further characterization and testing.

2.3. Carbonization and activation

The freeze-dried materials prepared in Section 2.2. were carbonized in a tube furnace at 500 °C at a heating rate of 5 °C/min and under nitrogen flow of 25 L/h. The samples were then dispersed in KOH solution for at least 10 h under stirring. Different ratios of KOH/Carbonized material = 1, 2, 3 and 4 were used to find the optimum condition for the generation of the desired pore structures. The KOH treated materials were vacuum filtered and oven dried at 60 °C. This was followed by activation in a tube furnace at 750 °C for 1 h at a heating rate of 5 °C/min and under nitrogen flow of 25 L/h. The samples were then washed with 1 M HCl solution and followed by washing with distilled water until the pH was around 7. The resulting materials were oven dried at 60 °C overnight and characterized by a combination of several analytical techniques.

2.4. Characterization

The Fourier transform infrared spectroscopy (FTIR) spectra were recorded on a Nicolet iZ10 FTIR spectrometer with attenuated total reflectance (ATR) accessory from 4000 cm^{-1} to 400 cm^{-1} to evaluate the chemical bonds and structures in the obtained materials. Spectra were averaged over 64 scans. The morphology of the synthesized nanoparticles and hierarchically porous materials was observed with a scanning electron microscopy (SEM) (Mira 3 LMH, Tescan Company). The samples were sputter-coated with a thin layer of gold prior to SEM observation. The accelerating voltage of Schottky cathode was 3 kV. Secondary electrons were detected by the Everhart-Thornley type secondary electron detector or by the in-lens detector (In-Beam). The average size of the PS nanoparticles was determined by dynamic light scattering (DLS, Malvern Zetasizer Nano). The same device was used to evaluate the zeta potential of the PS NPs through the Smoluchowski model. The thermal stability of the materials was evaluated by thermal gravimetric analysis (TGA) using an STA-780 series Thermal Analyzer (Stanton-Redcroft, UK) under nitrogen flow (20 mL min^{-1}) at a heating rate of 10 °C min^{-1} from room temperature to 850 °C. To assess the textural properties of the materials, i.e. porosities and pore size distribution, these were measured by Hg porosimetry using Micromeritics AutoPore IV 9500 analyzer. For the surface areas, conventional nitrogen isotherms at 77 K were measured using Nova 2200 e surface area analyzer (Quantachrome). From this analysis, surface areas were obtained from the Brunauer-Emmett-Teller (BET) equations. The total pore volumes were measured at the relative pressure of 0.985 and the pore size distribution was determined based on density functional theory (DFT) model. For a more accurate characterization of the micropores, CO_2 adsorption at 273.15 K was performed on all samples using a Quadrasorb-SI gas adsorption analyzer (Quantachrome, USA). Using the DFT model (based on statistics and provided by the software) and assuming slit pore geometry, the corresponding pore size distributions were computed. With this method, it is possible to access the ultramicropores (sizes < 1 nm). The surface areas from CO_2 sorption were based on the BET model and were computed using the data collected in the range of values of relative pressures P/P_0 from 0.013 to 0.019. All the samples were degassed under vacuum (0.1 mbar) at 115 °C for at least 10 h before the measurements. Elemental composition (C, H, N) of the samples was determined with an Elementar vario EL Cube analyser (Elementar, Germany). XPS measurements were done on Omicron Nanotechnology with monochrome radiation of Al lamp with energy 1486,7 eV in constant analyser energy (CAE) mode. Measured spectra were evaluated by software Casa XPS where after intensity calibration the area of peaks and relative sensitivity factors (RSF) from database are used for determination of concentrations.

2.5. CO_2 adsorption measurements

CO_2 adsorption measurements of the hierarchically porous materials were characterized using a Quadrasorb-SI gas adsorption analyzer (Quantachrome, USA) according to the procedure described in Beltzung et al.[28] Specifically, all the samples were degased at 115 °C for a minimum of 10 h to remove moisture and adsorbed gases from the pores before the measurements. The adsorption in moles per unit mass of adsorbent was calculated using the volumetric measurement and assuming ideal gas behavior at 1 atm and 273.15 K.

3. Results and discussion

3.1. Synthetic approach to the hierarchical porosity

The proposed strategy for designing the stable hierarchically porous materials was aimed at creating in the same material a range of pore sizes while retaining a good amount of nitrogen functionalities on the carbon framework, given its reported affinity towards CO_2. The creation of different pore sizes was necessary to facilitate efficient gas diffusion, while simultaneously enhancing the CO_2 adsorption capacity. Polyaniline (PANI), one of the most studied conductive polymers was selected as starting polymer, thanks to its high nitrogen content, easy synthesis and low cost [43–45]. The intrinsic presence of nitrogen in the molecule of aniline (the monomer), made it certain to have nitrogen groups homogenously distributed in the carbon based final materials. The spherical PS NPs were chosen as building blocks, based on their high glass transition temperature (T_g), which gave rigid and non-deformable support to the 3-D framework [42,46–49] and later on as sacrificial template. Upon carbonization and removal of PS NPs we expected to create additional pores and increase the surface area and pore volume of the final materials. In order to investigate the effect of crosslinking the polymer on the results of heat treatment and final CO_2 capture, PS coated PANI (P1) and PS coated crosslinked PANI (P2) were prepared. Similar synthesis was performed but without PS NPs and were named P3 (PANI) and P4 (crosslinked PANI) to demonstrate the importance of the PS NPs in the creation of the hierarchical porosity. The synthesis procedure is depicted in Scheme 1 for clarity. The carbonized materials treated at 500 °C were denoted P1_CAR, while the

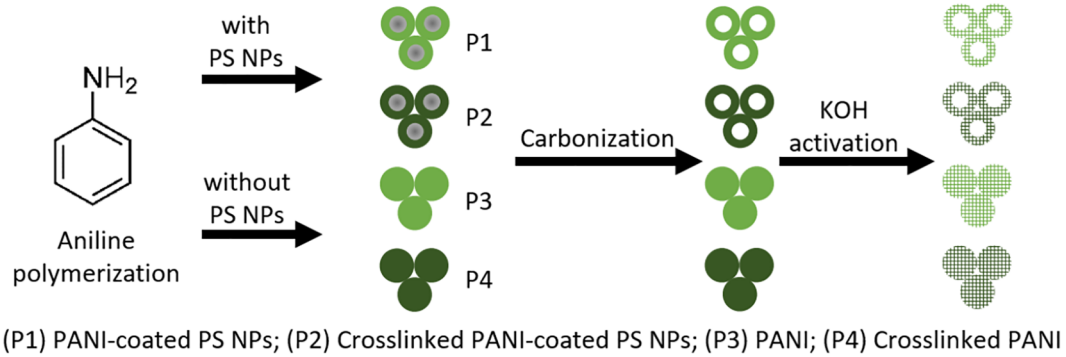

Scheme 1. Parameters for synthesizing the 3-D porous materials.

KOH activated samples were named P1_X, where X denotes the mass ratio between KOH and the pre-carbonized material (i.e. 1, 2, 3 or 4) used for the activation step.

3.2. Morphology and porous properties of the as-synthesized materials

Before the activation process, the as-synthesized materials showed a mesh-like structure indicating the growth of PANI nanostructures on the PS NPs support forming 3-D structures (Fig. 1a). The rigid monodisperse PS NPs preserved the outer PANI structure upon crosslinking without significant deformation or shrinkage (P2, Fig. 1b) exhibiting inter-particle channels. With the control samples prepared without PS on the other hand, a more globular structure with large grain sizes was obtained upon crosslinking (P3 and P4, Fig. 1 c and d) indicating limited porous structure. The large clusters of P3 and P4 are more prevalent at lower magnification (5 µm) (Fig. SI 1, Supporting Information). During the polymerization of aniline, the initiator solution was added slowly to control the polymerization rate such that PANI nanostructures get deposited onto PS NP building blocks forming a 3-D mesh-like structure. For comparison, we also prepared porous materials by addition of APS as a shot instead of slow addition. Obtained results confirmed that this approach led to the rapid polymerization of PANI forming larger granular structures instead of PANI nanostructures obtained from our standard approach (see Fig. SI 2, Supporting Information).

To track the evolution of the pore formation, the textural properties of the as-synthesized materials were evaluated by means of N_2 sorption at 77 K and Hg intrusion porosimetry. The surface areas were calculated using the Brunauer-Emmett-Teller (BET) equation, whereas the pore size distributions were calculated using the density functional theory

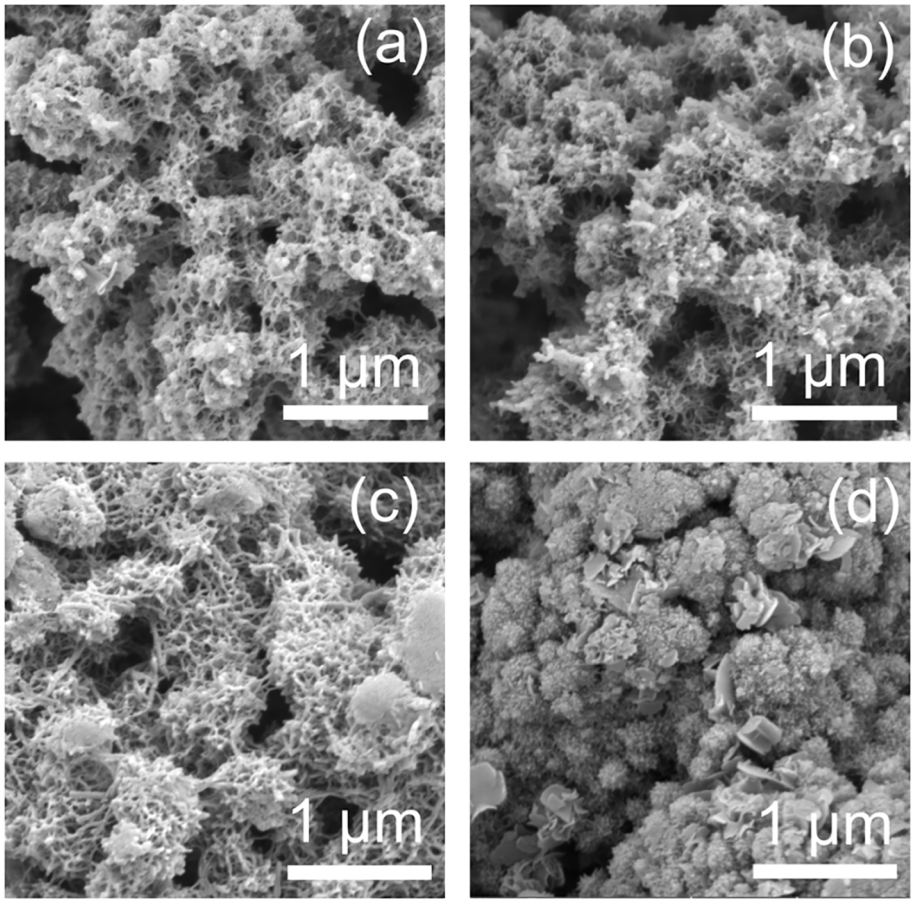

Fig. 1. SEM images of as-synthesized porous materials at 5 wt% solid content (a) P1 (b) P2 (c) P3 and (d) P4.

(DFT) from the N_2 adsorption isotherm. As shown in the N_2 sorption isotherms (Fig. SI 3 (a), Supporting Information), the as-synthesized materials before the chemical activation step all showed typical type II isotherm according to the Bruner-Deming-Deming-Teller classification [50,51], with low surface areas (S_{BET} < 32 m^2 g^{-1}), which corresponded to macroporous structures with low or inexistent microporosity. As the relative pressure increased above 0.6, there was a uniform increase in the uptake of nitrogen coupled with a minor hysteresis loop, which can be attributed to the mesoporosity. From the Hg porosimetry data, we observed clearly the hierarchical porosity for P1 and P2 with two different pore size ranges indicating the inter-particle meso- and macroporosity due to the presence of PS NPs. In the case of the samples prepared without PS NPs (P3 and P4), a single broad pore size distribution was observed (Fig. SI 3 (d), Supporting Information). As seen in Table SI 1 in Supporting Information, the porosity only decreased slightly from 87% in P1 to 85% in P2 upon crosslinking, which we believe was due to the rigid PS NPs maintaining the 3-D structure of the material. With the PS-free samples, the porosity decreased from 82% in P3 to 73% in P4, demonstrating the impact of PS NPs to maintain the 3-D structure, while avoiding the loss of porosity when the material was crosslinked.

3.3. Pore-generation: effect of carbonization and activation conditions on material properties

For the various sorbents that have been reported as the most promising in terms of CO_2 sorption performance, two main parameters have been identified as crucial for enhancing their performance: (1) optimized size of accessible pores usually below 0.7 nm and (2) presence of accessible surface functionalities on the porous material matrix, which can improve CO_2 uptake and selectivity. Generally, N-doped porous sorbents with different porosities, nitrogen and oxygen contents and sorption properties were obtained depending on the synthesis approach as well as the different carbonization and activation conditions used [6,52]. As such, the temperatures for carbonization and activation were selected to keep a balance between textural properties and surface chemistry based on similar investigations reported in the literature. Although higher pyrolysis temperatures could generally yield higher surface areas, it may also lead to a compromised opening up of narrow micropores with resulting increase in mesopore volumes and a loss in surface functionalities [13,15,53,54]. With the aim of generating a hierarchical pore structure with a high amount of micropores while also retaining a reasonable amount of surface functionalities, the as-synthesized materials were subjected to a first heating treatment at 500 °C at a rate of 5 °C min^{-1}. This step, known as the carbonization step, was important to slowly decompose the PS NPs and carbonize the PANI frameworks. Thermal gravimetric analysis (TGA) revealed a major decomposition between 400 and 500 °C (Fig. 2) which corresponded ~~s~~ to the degradation of PS NPs with the weight of PS NPs nearing 0%. This was followed by a chemical activation at 750 °C using potassium hydroxide (KOH). This is the most used agent for the activation of carbon materials due to its low energy demand and less impact on the environment when compared to other activating agents [6]. Its presence enhances the pore development process, for example, samples carbonized in the presence of KOH exhibited more developed porosity compared to samples carbonized in the absence of it, clearly indicating its role in formation of small pores [53]. During the KOH activation process, potassium ions are released, which intercalate into the amorphous part of the graphitic fingers of the carbon, reacting with it and producing large number of fine pores under high diffusion and pyrolysis action. This results in an increase in the surface area and pore volume [13,55]. We observed that the high surface hierarchically structured materials were only obtained after the activation step and there was no significant increase in surface area and pore volume of the materials after stopping at the carbonization step (Table SI 2, in Supporting Information).

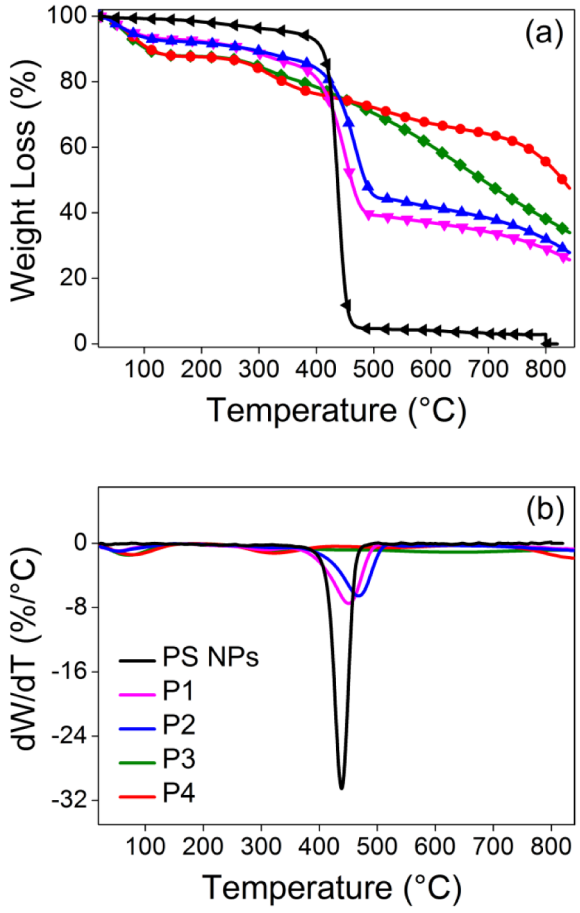

Fig. 2. Thermal behaviour of PS NPs and PANI microclusters measured by TGA under nitrogen atmosphere (a) Weight vs. temperature TG curve (b) DTG curve, derivative of the TG curves (▼) P1 = PANI-coated PS NPs; (▲) P2 = Crosslinked PANI-coated PS NPs; (◆) P3 = PANI; (●) P4 = Crosslinked PANI; (◀) PS-NPs.

Overall, a higher carbon mass remained for all the crosslinked materials in comparison to non-crosslinked materials (Fig. 2, Table SI 3 in Supporting Information). The weight difference is due to the thermal stability of the crosslinker, phytic acid, which undergoes dehydration and carbonization and therefore slightly increasing the weight of the crosslinked materials.

Examples of SEM images of the activated materials are shown in Fig. 3(a–d). It was observed that the skeleton of the PS-PANI microclusters contain interconnected spherical pores left by the removal of PS NPs, which created additional porosity for easy diffusion of CO_2 (see Fig. 3(a) and (b)). Comparatively, as shown in Fig. 3(c) and (d), the PANI microclusters prepared without PS NP building blocks showed globular rather than the hierarchically porous structures.

The formation of the high surface area hierarchically porous materials after the carbonization and activation steps was further confirmed by the change in the adsorption isotherms from type II to type I (Fig. SI 4, Supporting Information), typical of microporous materials with significant adsorption at low relative pressures. Moreover, transmission electron microscopy (TEM) images of the optimum material are presented in Fig. 4, clearly showing the porosity of the carbon, which is important for efficient gas diffusion.

Using various KOH/C ratios (1, 2, 3 and 4) for activation, a series of nitrogen-doped carbons were produced where the textural and surface chemistry were well tuned. It was observed that treatment with the KOH/C ratio of 1 mostly resulted in non-microporous materials with low surface areas. This may be due to the less efficient pore generating process at low KOH amounts resulting in predominantly mesoporous

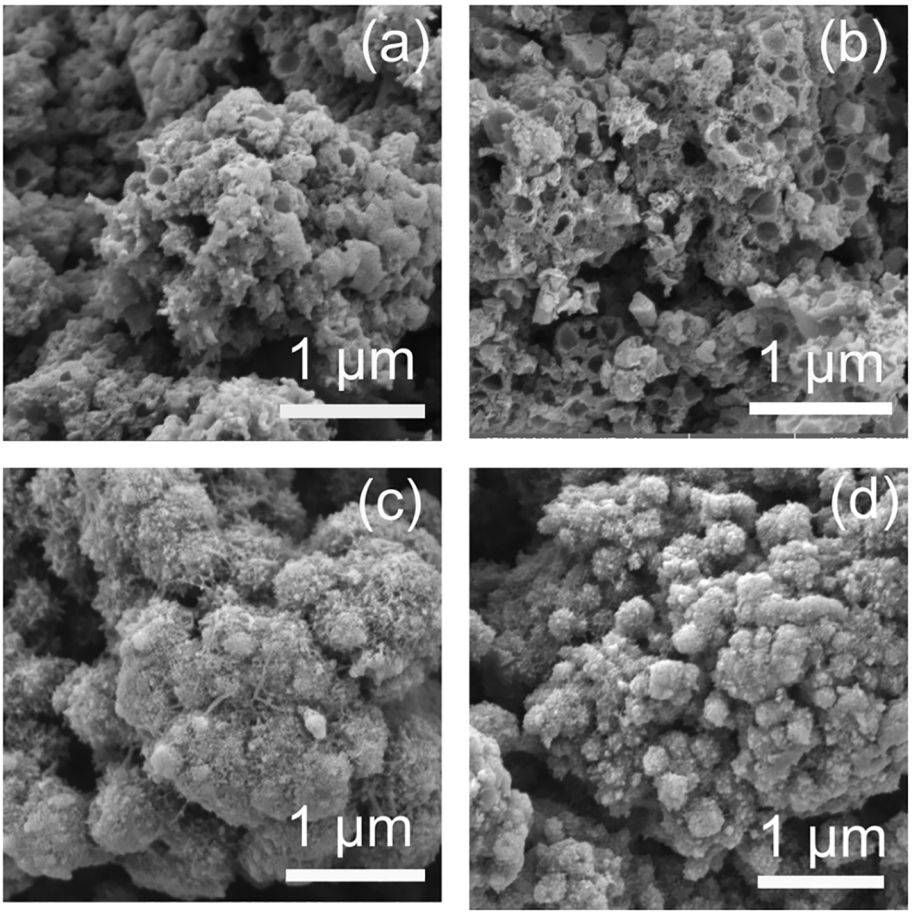

Fig. 3. SEM images of KOH activated materials (a) P1 (b) P2 (c) P3 (d) P4, magnification = 50 kX.

materials. Generally, the lower KOH/C ratios lead to less efficient pore generation whereas too high KOH/C ratios result in harsh activation and the resultant pore widening or degradation of the 3D structure. It was therefore concluded that this ratio was not sufficient to generate the desired micropore sizes for CO_2 capture. Samples treated with KOH/C ratios of 2, 3 and 4 were highly microporous to various degrees depending on their composition with enhanced surface area and pore volume. The high N_2 uptake of the activated samples at low relative pressures $P/Po < 0.01$ confirmed the predominantly microporous nature of the materials (IUPAC definition pore diameters < 2 nm). Moreover, the isotherms showed slight hysteresis loops (type H4), indicating the presence of some mesopores. This was also clearly reflected in their corresponding pore size distributions (PSDs) obtained by the non-local density functional theory (NLDFT) shown in (Fig. SI 4 (b), (d) and (f), Supporting Information). Complete report of the measured specific surface areas, total volume and average pore diameter are reported in Table SI 2 in Supporting Information. Although the activated materials also contain ultramicropores (with pore diameters < 0.7 nm), they were too narrow for N_2 to diffuse into them at 77 K. As such these were not optimally determined using N_2 sorption as evidenced by the incomplete pore size distributions in the micropore range. These smaller pores were subsequently evaluated from CO_2 sorption analysis.

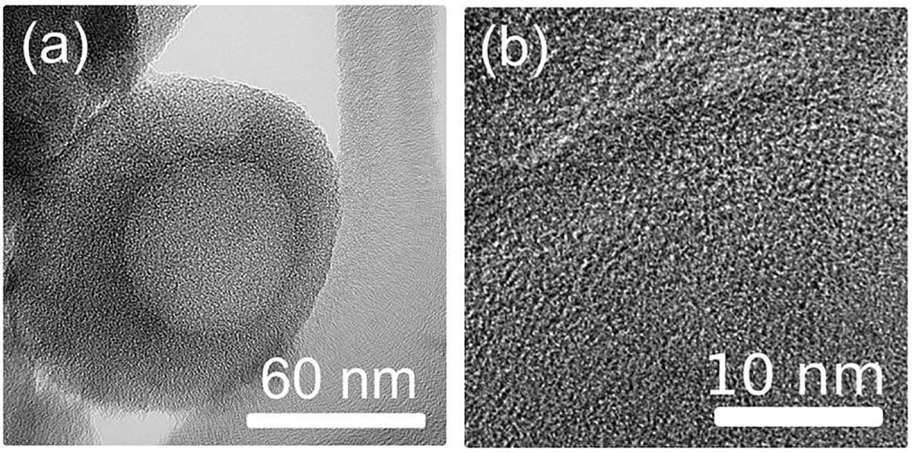

Fig. 4. TEM images of the optimum porous carbon P2_3 with two different magnifications.

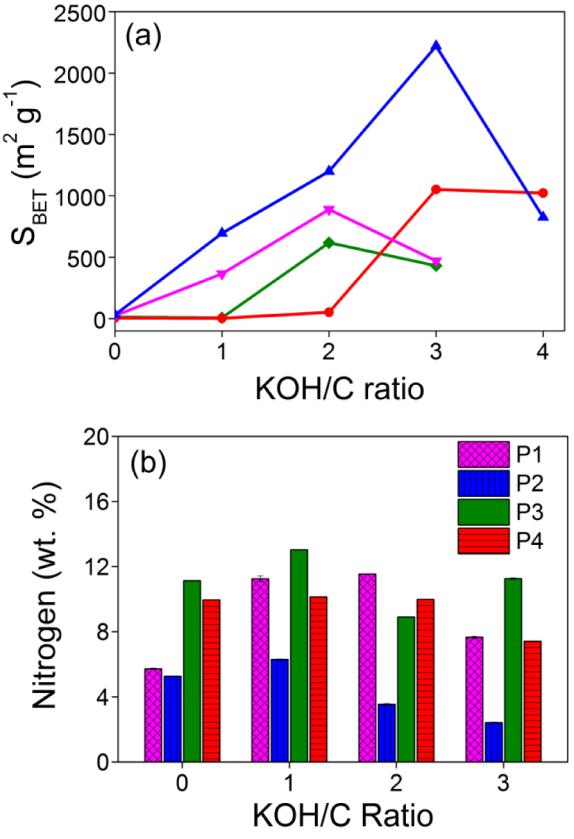

Fig. 5. (a) Trend in the evolution of BET surface areas of the microclusters obtained from N_2 sorption and (b) Nitrogen content in relation to KOH/C ratio (▼) P1 = PANI-coated PS NPs; (▲) P2 = Crosslinked PANI-coated PS NPs; (◆) P3 = PANI; (●) P4 = Crosslinked PANI.

The trend in evolution of BET surface areas with different KOH treatments as displayed in Fig. 5(a) showed that increasing the KOH/C ratio from 1 to 3 resulted in the formation of new pores and thus to higher surface areas. This effect was more pronounced for the materials, which were crosslinked with phytic acid. The phytic acid networks ensured maximum KOH adsorption of the carbonized material, and thus a well-developed porosity in the subsequent activation step due to the pore-generation property of KOH [13]. When the ratio KOH/C 4 was used for the crosslinked materials, we observed a generation of wider pores with an increase in the average pore sizes (Fig. SI 5 (a and b) in Supporting Information, BET results in Table SI 2), which was in line with previous reports which indicated the generation of too large pores and almost complete removal of nitrogen functionalities when KOH/C ≥ 4 were used for activation [13,22,32]. Even though the sample P4 treated with KOH/C = 4 did not show a huge decrease in BET surface area compared to sample P2 treated with KOH/C = 4, the SEM images confirmed the creation of large pores. From these results, the KOH/C ratio of 3 was the optimum condition for the crosslinked materials.

For the non-crosslinked samples, increasing the KOH/C ratio from 1 to 2 resulted in a significant increase in the surface area whereas a further increase of KOH/C to 3 resulted in a huge decrease in the surface areas. The reason for such observation is likely due to weaker structure in the absence of phytic acid leading to the complete destruction of the 3-D structure at higher KOH amounts (Fig. SI 5 (c), Supporting Information), with a corresponding decrease in the surface areas and pore volumes. As such, the optimum treatment for the non-crosslinked materials was KOH/C ratio of 2. The final hierarchically porous materials exhibited an optimized N_2 BET surface area of up to 2200 m^2 g^{-1} (P2) and total pore volumes as large as 1.21 cm^3 g^{-1} (P2) with pore diameters < 1.8 nm. The difference observed in surface areas and pore volumes of the porous materials as prepared, after the carbonization and KOH activation steps, was an evidence of the role of KOH in the generation of high number of micropores (See Table SI 2, Supporting Information for the detailed textural properties).

Previous investigations have indicated a strong link between N-functional groups and CO_2 sorption capacity. Therefore, the nitrogen content of the prepared materials was analyzed by organic elemental analysis as shown in Fig. 5(b). All the materials retained high amounts of nitrogen reaching up to ~13 wt% after the activation step, which was far higher compared to similar materials prepared through chemical activation methods [13,38]. Apart from the material composed of pure PANI, generally, the nitrogen content decreased with an increase in the KOH/C ratio, which is in agreement with previous reports [22,53]. It was observed that the nitrogen content of the carbons before KOH treatment was lower than the nitrogen content of materials treated with KOH/C = 1. The reason for this observation was the change of the material composition during the thermal treatments. Throughout the material treatments from carbonization up to KOH activation, certain groups (O, C and N groups) were removed from the polymer structure causing the overall N content, which was calculated based on the total number of elements, to increase. Moreover, comparing the carbon, hydrogen and nitrogen content before and after activation indicated that the activation process altered the groups to different degrees for each sample without any trend, which could be due to the heterogenous distribution of the groups on the surface with some embedded in the bulk of the material. The full elemental composition of the as-synthesized and activated samples under different KOH/C treatments is shown in Table SI 4 in Supporting Information. The optimized material (P2_3) obtained at the highest KOH/C ratio of 3, however had the lowest amount of nitrogen because of the opposite effects of the activation conditions on microporosity and nitrogen content [11,19,22].

3.4. Chemical structure by FTIR-ATR spectroscopy

In order to understand the structural changes of the materials during the thermal treatment process, the evolution of the structure was studied using FTIR-ATR. The FTIR spectra of the as prepared, carbonized and activated materials are shown in Fig. 6, where “CAR” and “ACT” after the name P1-4 are abbreviations of carbonized and activated, respectively. The characteristic absorption bands at about 1518 and 1620 cm^{-1} were observed for all the materials. This corresponded to the carbon-carbon aromatic ring stretching vibrations of benzenoid and vibration of quinoid rings of PANI, respectively. The band at 1340 cm^{-1} was attributed to the C—N stretching vibrations of secondary aromatic amines and the peaks at 1194 and 843 cm^{-1} are noted for the C—H in-plane and out-of-plane bending. The fact that similar peaks were observed in all the PANI and PS-PANI microclusters was an indication that the PS NPs were uniformly covered by PANI. After carbonization at 500 °C, the two main peaks assigned to the benzenoid and quinoid rings broadened and became weaker and less sharp, which was due to the strong absorption of carbon [22]. The disappearance of the maximum peak at 1194 cm^{-1} was due to the deprotonation of the materials at high temperatures. In the activated samples, the broad peak with maximum at 1677 cm^{-1} corresponded to the G band (graphite-like structure) of carbon [56]. The spectrum of the final activated samples confirmed the synthetic approach resulting in the conversion of the polymeric material to carbon. It was also observed that the C—N absorption band decreases as the materials are carbonized and activated, hence highlighting the loss of some of these functional groups during these latter treatments. In order to follow quantitatively the evolution of nitrogen, oxygen and carbon atoms before and after activation, XPS analysis was carried out as reported in the subsequent sections of the manuscript (Section 3.6.3).

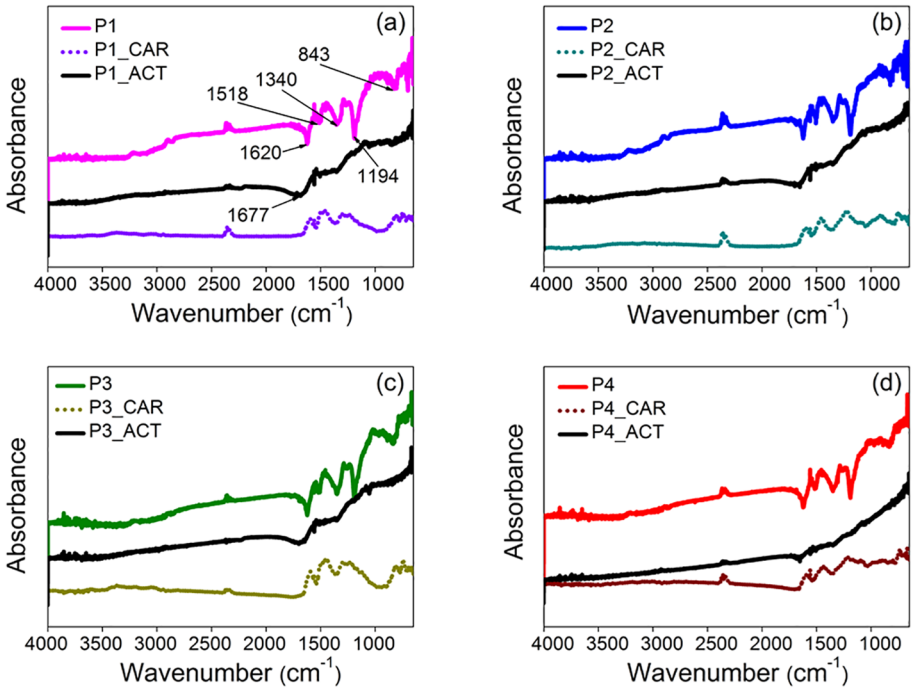

Fig. 6. FTIR spectra of the materials as-synthesized carbonized at 500 °C and activated at 750 °C. CAR and ACT after the sample names are abbreviations for carbonized and activated respectively.

3.5. CO_2 capture performance

Due to the creation of abundant micropores and the high amounts of nitrogen functionalities measured in the prepared materials, their CO_2 sorption capacities were evaluated. The CO_2 capacity was evaluated by measuring the entire adsorption isotherm at 1 atm and at 273.15 K by volumetric method. This pressure (1 atm) was used because post-combustion CO_2 capture is typically carried out at low pressures. To estimate the values of uptake of CO_2 in mmol g^{-1}, the highest values of adsorbed volume have been considered assuming ideal gas behavior. The CO_2 sorption capacity measured at 273.15 K and 1 atm also enabled the evaluation of the narrow micropores, since these were not properly obtained in the N_2 sorption measurements. An example of the CO_2 sorption isotherms measured for four optimally performing samples in each sample class are presented in Fig. 7(a). Complete results for the different KOH/C ratios and their corresponding pore size distribution (PSD) curves are shown in Fig. SI 6 and 7 in Supporting Information. All the isotherms displayed type I curves with slight hysteresis loops indicating the presence of both micropores and mesopores. The corresponding PSD curves in Fig. 7(b) showed that all the materials possess a significant amount of micropores ranging from 0.3 to 1 nm, with a maximum around 0.5–0.6 nm.

With the exception of materials activated at KOH/C = 1, all the other materials exhibited high CO_2 sorption capacities, which pointed to the fact that the CO_2 capture capacities were closely related to the narrow microporosity of the carbons, which was developed at KOH/C of 2 and 3. The results are summarized in Table 2 or its graphical representation in Fig. SI 8, Supporting Information).

For the crosslinked materials (P2 and P4), the higher the KOH/C ratio, the higher the surface area and pore volume, and the higher the corresponding CO_2 capacity. For the non-crosslinked materials (P1 and P3), at the optimum KOH/C of 2, the highest CO_2 sorption capacity was obtained. When the KOH/C ratio increased to 3, it resulted in a decrease in the surface areas and pore volumes with a corresponding decrease in the CO_2 capture capacity. This trend was in good agreement with that observed in the case of surface areas in Fig. 5(a). The textural properties (obtained from CO_2 sorption data), and CO_2 adsorption capacities of the

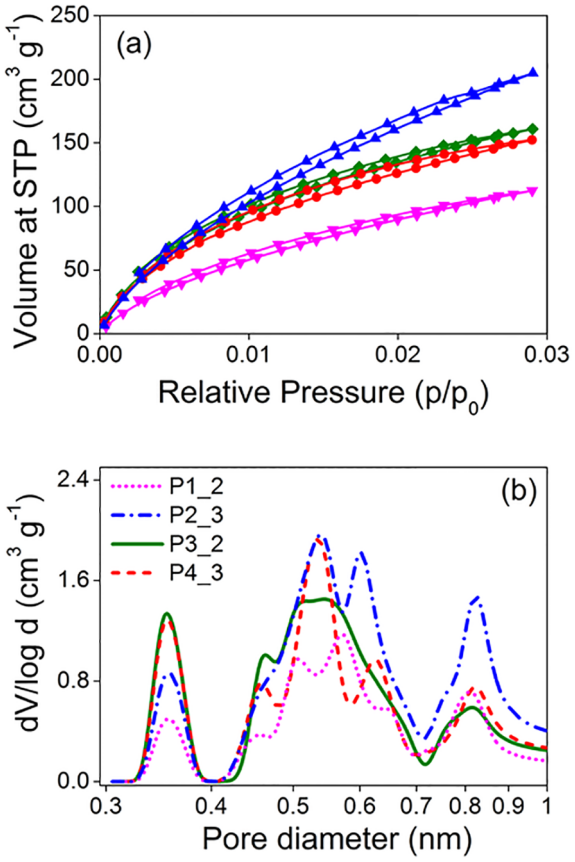

Fig. 7. (a) CO_2 adsorption and desorption isotherm of the optimum material at 273.15 K and 1 bar (b) Corresponding pore size distribution (▼) P1_2; (▲) P2_3; (◆) P3_2; (●) P4_3.

Table 2
Textural properties and CO_2 capacities of the materials measured at 273.15 K and 1 bar.

Material	S_{BET} from CO_2 [$m^2 g^{-1}$]	Total V_{pore} (CO_2) [$cm^3 g^{-1}$]	V_{pore} for pores < 0.7 nm [$cm^3 g^{-1}$]	CO_2 Capacity [mmol g^{-1}]
P1_1	524	1.19	0.13	3.02
P1_2	1080	2.35	0.21	5.02
P1_3	717	1.66	0.17	4.02
P2_1	1115	2.47	0.22	5.15
P2_2	1537	3.24	0.27	6.50
P2_3	2036	4.36	0.39	9.14
P3_1	309	0.62	0.09	2.23
P3_2	1280	2.90	0.30	7.18
P3_3	700	1.58	0.18	4.21
P4_1	309	0.75	0.06	1.38
P4_2	427	0.95	0.12	2.72
P4_3	1219	2.81	0.29	6.80

Table 3
Textural properties, nitrogen content and CO_2 sorption capacity of our optimum materials in comparison to those reported in the literature measured at similar conditions (1 bar, 273 K).

Material (Sample name)	S_{BET} from N_2 [$m^2 g^{-1}$]	V_{total}[a]/[V (ultramicropore)[b]]	N content [%]	CO_2 Capacity [mmol g^{-1}]	Ref.
NC-800	263	0.38	5.58	2.65	[57]
SG–MOP-5	807	2.80	38.1	3.37	[58]
S3	390	–	6.82	3.56	[28]
SU-AC-400	4196[c]	2.26/[0.25]	0.55	4.30 (298 K)	SI of [13]
1000CDC	1887	–	2.5	4.67	[59]
HMT-80-900	809	0.34	2.0	5.6	[8]
600-2	2003	1.2	8.95	7.30	[11]
CS*-P-A	2400	1.07/0.27[d]	0	8.90	[32]
P3_2	618	0.35/[0.30]	8.9	7.18	This work
P2_3	2220	1.21/[0.39]	2.42	9.14	This work

[a] Total pore volume obtained from N_2 sorption at 77 K.
[b] The pore volume of ultramicropores (pores < 0.7 nm) was obtained from CO_2 sorption data at 273 K.
[c] S_{BET} evaluated from Ar adsorption at 87 K and P/P_o = 0.999.
[d] Cumulative pore volume calculated in the range up to 0.8 nm, the nitrogen content (N %) is obtained by elemental analysis

hierarchically porous materials are presented (Table 2). Overall, all the materials possess a high amount of micropores below 1 nm with high cumulative ultramicropore (pores with diameters < 0.7 nm) and corresponding volumes ranging from 0.12 to 0.39 $cm^3 g^{-1}$. The comparison of CO_2 sorption capacity of two of our optimum materials with the highest-performing materials in the literature is presented in Table 3.

It was observed that the CO_2 capture capacity of our best sample, P2_3 at 1 bar is among the highest reported values for most carbon materials. It is believed that the high CO_2 capacity of the materials at low pressure was mainly due to the synergistic effect of the hierarchical porosity (ultramicropores, mesopores and macropores in the same material). This facilitates the efficient diffusion of CO_2 for easy accessibility to the micropores, coupled with the high CO_2 adsorption in the ultramicropores.

3.6. Effects of textural properties and surface chemistry on CO_2 capture capacity

The contribution of textural properties and surface chemistry (nitrogen functionalities) to the CO_2 sorption performance of various porous sorbents has been debated by many researchers [32,36]. Gas physisorption is generally believed to be directly influenced by large specific surface areas and high pore volumes of adsorbents [54]. However, recent studies of some solid sorbents have revealed that high surface areas and large pore volumes do not necessarily lead to high uptake capacity [19,27]. While many reports have indicated the strong influence of surface chemistry of activated carbon on adsorption capacity, with enhanced CO_2 uptake upon nitrogen doping [6,25,60,61], a few other works have reported the opposite that nitrogen functionalities do not influence CO_2 adsorption under conventional operation conditions of temperatures 0–25 °C and pressures between 0 and 1 bar [32,36]. Overall, the most efficient CO_2 sorbents reported were those exhibiting two main characteristics: large number of properly sized narrow micropores to enhance efficient CO_2 uptake coupled with nitrogen functionalities in the structure to improve CO_2 affinity [10,22,62,63]. To understand the influence of the textural properties and surface chemistry on the CO_2 capture capacity of the materials, the CO_2 adsorption capacities were correlated with the textural properties (obtained from CO_2 sorption data) and the nature and content of nitrogen functionalities of the materials (obtained from organic elemental analysis).

3.6.1. Effect of pore sizes on CO_2 capture capacity

It was observed that there was no direct relationship between the BET specific surface area obtained from CO_2 sorption data and the CO_2 adsorption capacities (Table 2). Because the BET equation does not describe the CO_2 adsorption at 273.15 K most appropriately, the use of BET equation for evaluating surface areas resulted in a much lower surface areas than those obtained from N_2 sorption at 77 K (See Table SI 2 in Supporting Information). However, these values were evaluated in the same manner and were therefore used as a comparison among the different samples. Application of the Langmuir model in evaluating the surface areas was avoided because it can lead to overestimation of the surface area especially in this case, where the adsorption is not strictly by monolayer.

Although no direct relationship was observed between the specific surface area and the CO_2 sorption capacities, the sorption capacity was strongly correlated with the ultramicropore volume especially pores between 0.3 and 0.7 nm (considering that the kinetic diameter of CO_2 is 0.33 nm). In fact, the best performance in terms of CO_2 sorption capacity (9.14 mmol g^{-1}) was correlated with the highest ultramicropore volume of 0.39 $cm^3 g^{-1}$. Additionally, among the optimum materials, the sample P3_2 with the second highest sorption capacity exhibited the second highest ultramicropore volume of 0.3 $cm^3 g^{-1}$ compared to P2_2 (0.27 $cm^3 g^{-1}$) although P2_2 (1537 $m^2 g^{-1}$) had a higher specific surface area than P3_2 (1280 $m^2 g^{-1}$). Similar effect was seen in the case of P3_1 and P4_1, which both show the same specific surface area of (309 $m^2 g^{-1}$) but different microporosity, where P3_1 showed higher pore volume between pore size range of 0.3 and 0.4 nm than P4_1. This suggested that the micro and narrow mesopores were mainly responsible for the high CO_2 sorption performance of the materials at low pressure. It was interesting to note that when plotting CO_2 sorption capacity as a function of ultramicropore volume for all prepared materials, a linear relationship was observed (Fig. 8), confirming the strong influence of the ultramicropores in enhancing CO_2 capture. This linear correlation of CO_2 sorption capacity at low pressure with ultramicropore volume is in agreement with previous reports [13,36]. The enhanced uptake of CO_2 with higher ultramicropore volume has been attributed to increasing adsorption potential with decreasing pore width, resulting in complete filling of narrow micropores at low relative pressures.

3.6.2. Effect of nanoparticle size on the porous material properties

To further tune and evaluate the impact of pore sizes, we selected the optimum sample and condition for the activation (P2 activated using KOH/C = 3 at 750 °C) and evaluated the effect of the

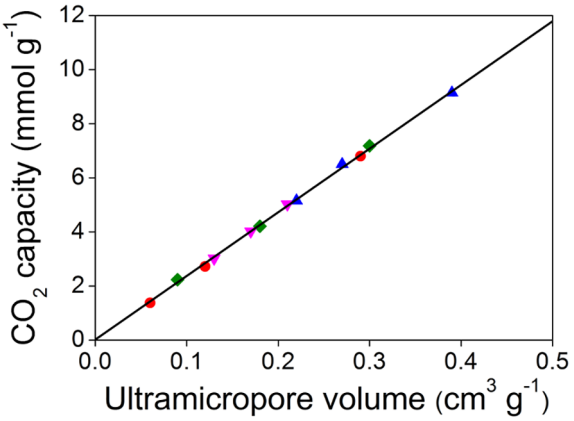

Fig. 8. Trends in ultramicropore volume (pores < 0.7 nm) in relation to CO_2 capture capacity; ratio (▼) P1 = PANI-coated PS NPs; (▲) P2 = Crosslinked PANI-coated PS NPs; (◆) P3 = PANI; (●) P4 = Crosslinked PANI. Line represents the best fit to the data.

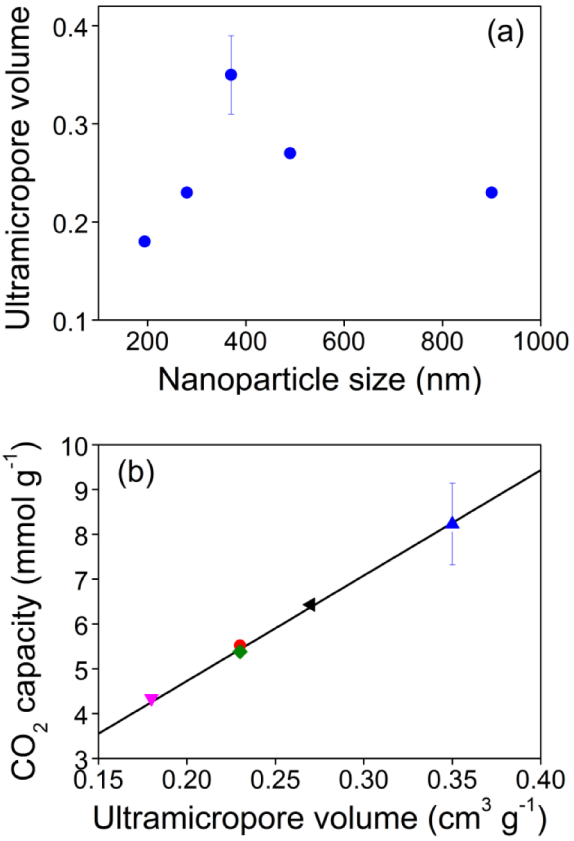

Fig. 9. (a) Effect of nanoparticle size on ultramicropore volume and (b) relationship between the ultramicropore volume and CO_2 sorption capacity (▼) 194 nm; (●) 280 nm; (▲) 370 nm; (◄) 490 nm; (◆) 900 nm, Line represents the best fit to the data.

nanoparticle sizes on the pore properties and subsequently on the CO_2 sorption capacity. Interestingly, the ultramicropore volume increased with increasing size of the particles up to an optimum of 370 nm and then a further increase in the size resulted in the decrease in the ultramicropore volumes (see Fig. 9 or the sorption isotherms depicted in Fig. SI 9 and the textural properties in Table SI 5, in Supporting Information). The observed trend could be due to the fact that with increase in the nanoparticle sizes, the porosity increases enabling effective KOH penetration for micropore generation. However with too large pores, the carbonization step, which removes PS NPs leaves very large pores. This most probably caused at least partial collapse of the hierarchical structure and the drop in the ultramicropore volumes. Similar to the trend observed in Section 3.6.1 and Fig. 8, the CO_2 capture capacity was linearly correlated to the ultramicropore volume (Fig. 9b), once again confirming the strong influence of this parameter on CO_2 capture capacity.

3.6.3. Effect of surface functionalities (nitrogen and oxygen) on CO_2 capture capacity

The CO_2 adsorbents prepared in this work consist mainly of nitrogen and oxygen atoms on the surface of carbon; therefore we investigated the effects of nitrogen and oxygen on the CO_2 capture capacity. The nitrogen content of the microclusters were quantified by organic elemental analysis (Table SI 4 in Supporting Information) and correlated to the sorption capacities of the materials. There was no obvious trend between the CO_2 capacity and the total nitrogen content of the microclusters (Fig. SI 10, Supporting Information). Although the sample P3_1 had the highest nitrogen content (13.03 wt%), its sorption capacity was far lower than the optimum material, P2_3, which had only 2.42 wt% of nitrogen. Considering the fact that the sample with the highest CO_2 sorption capacity had the lowest amount of nitrogen, this led us to conclude that at low pressures, the CO_2 capture behavior was mainly controlled by adsorption in narrow micropores, with no evidence on the contribution from the surface chemistry.

To further understand the contribution of the chemical interactions towards the high CO_2 sorption, XPS analysis was carried out on the optimally performing materials in each class to study the nature of the specific surface groups. Fig. SI 11 in Supporting Information shows the full XPS spectrum of the materials with three main peaks at binding energies of 284.98, 399.38 and 531.78 eV corresponding to carbon (C), nitrogen (N) and oxygen (O), respectively. The high resolution C1s spectra (Fig. 10) comprised of five different overlapping peaks at binding energy 284.7 eV showing presence of sp^3 carbon (−C−C−), 287.0 eV (−C−O(N)−), 288.3 eV (−C═O), 289.2 eV (−O−C═O) and 285.7 eV sp^2(−C═C−). Generally, all the samples presented the same type of carbon functionalities, with graphitic carbon being the major component.

Quantitative XPS analysis of the nitrogen groups revealed that P1, P2, P3 and P4 contained 5.45, 5.89, 9.39 and 6.62 wt% of total nitrogen, respectively. Although the amount of nitrogen reduced upon activation, all the samples retained a good amount of the nitrogen functionalities considering the amount in the as-synthesized samples (Table 4). These values were lower than those obtained by organic elemental analysis (Table SI 4, Supporting Information). The slight difference was due to the fact that XPS evaluates only surface nitrogen groups while organic elemental analysis takes into account the bulk nitrogen fraction. N1s core spectra allows us to obtain a better understanding of the types and local environment of the nitrogen atoms present in the material. The deconvoluted N1s spectra (Fig. 11) revealed the bonding of N with C and the existence of 4 types of nitrogen at the following binding energies: 399.3 eV (amine, $-NH_2$), 400.7 eV (pyrrolic, −N−H) 398.3 eV (pyridinic, ═N−H) and 401.6 eV (quaternary/graphitic, $=N^+-H$) present in all the activated samples as illustrated.

The relative peak areas of each nitrogen species arranged in order of highest CO_2 sorption capacity to the lowest are summarized in Table 4. It was observed that for all materials analyzed, the amine and pyrrolic nitrogen groups were the most stable and abundant, and could contribute to the high CO_2 capture. Similar to our findings, many researchers have identified the pyrrolic or amine nitrogens to have stronger interactions with CO_2 molecules [15,20,21]. Although there was no obvious contribution from nitrogen functionalities, it is worth noting that because of the tendency of gas desorption at higher temperatures, microporous materials without any CO_2-philic sites present may not be appropriate for practical CO_2 capture applications [7,21,64]. Moreover, it was recently reported by Xing et al. [19] that

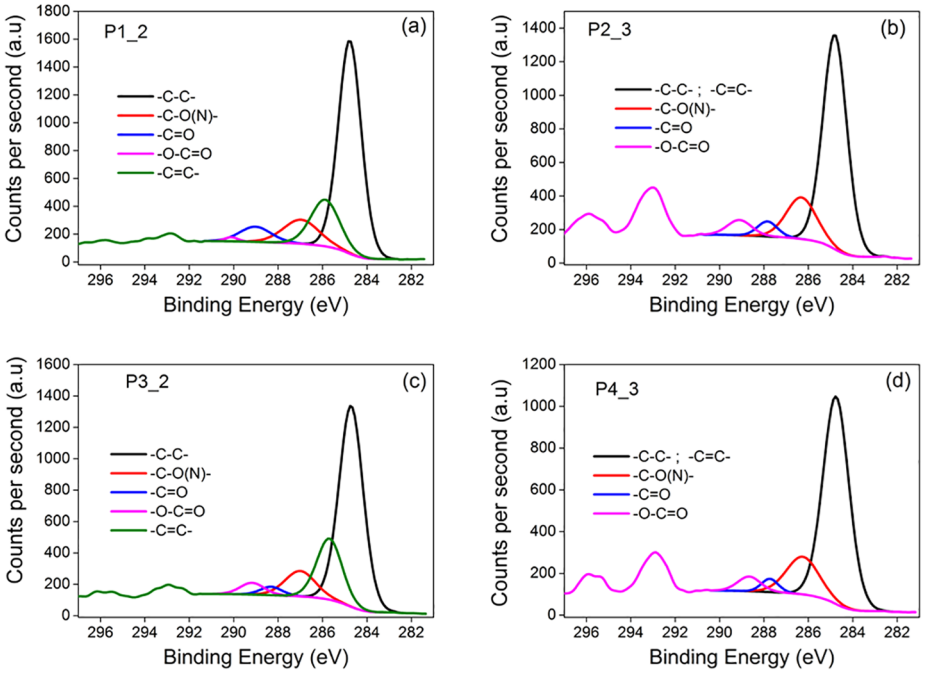

Fig. 10. C 1s core-level spectra of the activated carbons.

the CO_2 capture capacity of carbons can be further increased by an additional interaction. They found that the introduction of nitrogen into carbon facilitated hydrogen-bonding interactions between the carbon surface and CO_2 molecules, accounting for high CO_2 uptakes. This could explain why the presence of even a small amount of nitrogen (2.42 wt% measured by elemental analysis) in our optimized material (P2_3) could contribute to the high CO_2 sorption capacity significantly. However, this phenomenon needs further investigation.

As the surface oxygen functionalities on the surface have also been indicated to contribute to enhanced CO_2 sorption [65], the oxygen content detected from XPS was correlated with the CO_2 sorption capacity of the optimum materials (Fig. 12a). Although there was no obvious trend between the oxygen content and the CO_2 sorption capacity, it was observed that for all materials, the oxygen content was higher than the nitrogen content (Fig. 12b). Comparing the oxygen content before and after activation (Fig. 12c) indicated that the activation process altered the oxygen content to different degrees for each sample, which could be due to the heterogenous distribution of oxygen on the surface. Additionally, an attempt was made to ascertain whether there was an optimum N/O ratio, which favoured high CO_2 uptake. From Fig. 12(d), No correlation was observed with N/O ratio, this again could be due to the heterogenous distribution of oxygen in the surface and bulk. Similar to these results, He et al.[13] found no correlation between CO_2 sorption capacity and the oxygen content of their materials.

3.7. Considerations for industrial applications: sorbent regeneration

In designing a low-cost CO_2 capture sorbent that can replace aqueous amine-based CO_2 capture systems. The sorbent should (i) be prepared from cheap materials by a simple approach, (ii) have a hierarchical pore structure for high adsorption capacity and efficient diffusion, (iii) be mechanically and thermally stable and (iv) exhibit a minimum CO_2 capture capacity of 2–3.0 mol/kg of sorbent and high CO_2/N_2 selectivity, (v) be easily regenerable and with minimal or preferably no environmental impact to enable wide-scale application [3,7,41,66].

So far, the most important technological challenge for large scale application of post-combustion CO_2 capture to industrial units is the potential to lower the costs of capture. Therefore, sorbent regeneration capability is very crucial as it determines the lifetime and replacement frequency of the sorbent, which affects the overall cost of capture. In this regard, porous carbons are advantageous compared to other solid sorbents because they are easily regenerated. Fig. 13 shows the CO_2 sorption capacities per cycle of the optimized sample (P2_3) for eight subsequent cycles with simple vacuum regeneration at 115 °C after each cycle. The detailed textural properties and the sorption isotherms are shown in Table SI 6 and 7 and Fig. SI 12 and 13 respectively. To consider realistic deviation between repetitions, the sorption capacity graph is accompanied with the error bars, which were calculated for first four cycles as 2x standard deviation, thus considering 95% confident interval. Due to lack of repetitions for 5 to 8 cycles, these were estimated as an average of the error bars calculated for first 4 cycles.

Table 4
Proportion of oxygen content and nitrogen types (N1s) from XPS spectra of the as-synthesized and activated materials.

Material	Total oxygen as-prepared	Total oxygen-activated	Total N[a] [wt. %]	Total N[b] [wt. %]	PLN [%]	PDN [%]	QN [%]	NH [%]
P2_3	16.73	19.28	5.89	1.90	23.24	17.88	22.16	36.72
P3_2	10.12	8.68	9.39	7.58	15.75	15.55	15.54	53.17
P4_3	15.96	19.01	6.62	6.08	32.89	24.53	15.19	27.39
P1_2	18.00	10.96	5.46	4.36	44.18	22.81	15.35	17.67

[a] Nitrogen content in the as-synthesized materials.
[b] Nitrogen content in the activated materials, PLN (Pyrrolic nitrogen at position 400.70 eV), PDN (pyridinic nitrogen at 398.27 eV), QN (Quaternary Nitrogen at 401.63 eV) and (NH) amine at position 399.33 eV.

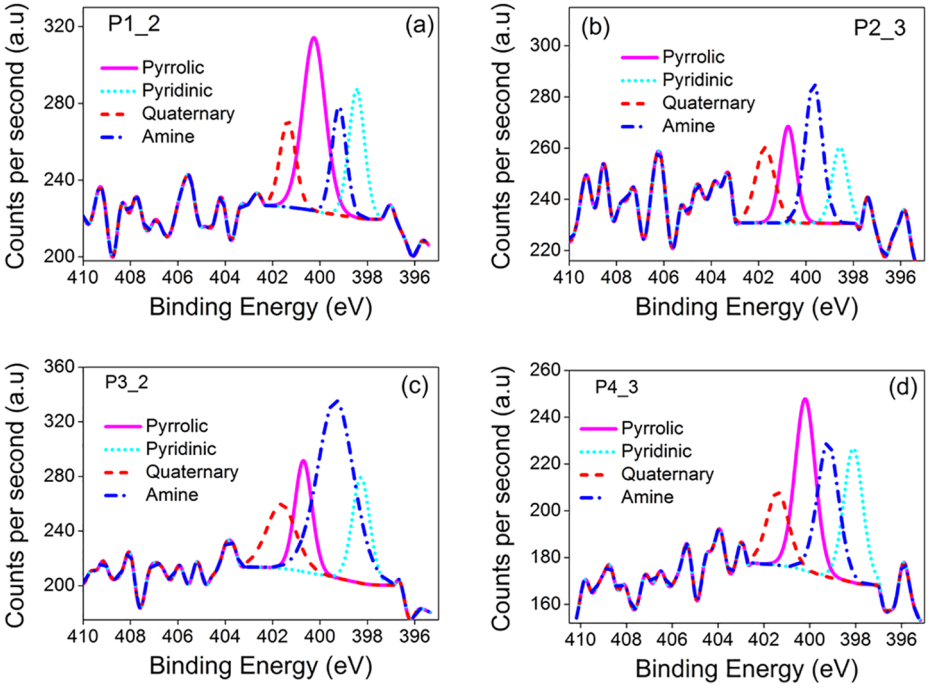

Fig. 11. N 1s core-level spectra of the activated carbons.

Based on the obtained results of regeneration, we observed the highest reduction in sorption capacity after the first cycle, whereas further cycles within statistical uncertainty of the measured data did not show significant reduction of the sorption capacity. From the CO_2 sorption isotherms measured after each regeneration cycle (Fig. SI 13), we observed a change in PSD after the first regeneration while other distributions were rather similar to each other independent on the number of regeneration cycle. There was no significant difference in the chemical composition of all tested materials (see Fig. SI 14 and 15) indicating that physical adsorption in ultramicropores (physisorption) is the main binding mode. However, the loss in sorption capacity, despite no change in composition suggested that there were small changes to the material porosity. In fact, when plotting all measured data of CO_2 sorption capacity as a function of ultramicropore volumes including regeneration cycles, all of them follow the same linear relationship (Fig. SI 16 in Supporting Information).

Practically, since the binding mechanism of our materials is only by physisorption, we believe this requires lower amount of energy for regeneration compared to aqueous amine absorption process, where CO_2 is reacting with amine molecules (chemisorption). In addition, it was

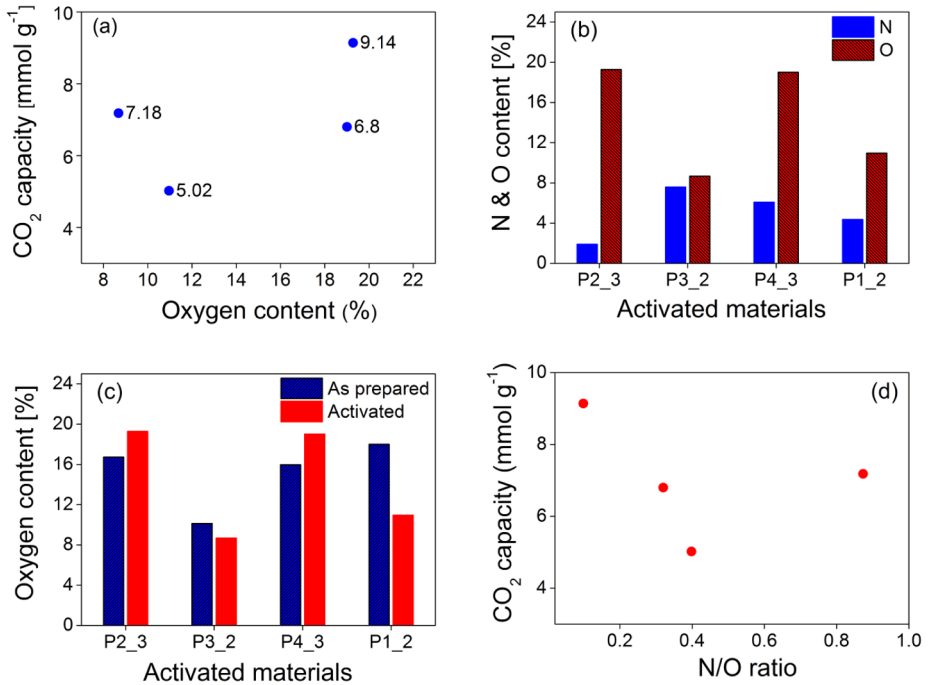

Fig. 12. (a) Effect of oxygen content on CO_2 capacity (b) comparison between nitrogen and oxygen content (c) effect of activation on oxygen content (d) effect of N/O ratio on CO_2 capacity.

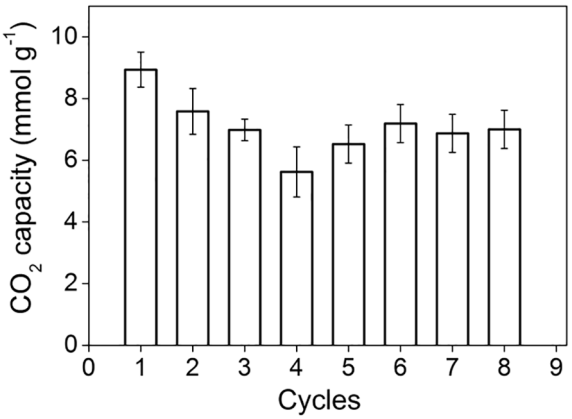

Fig. 13. (a) CO_2 capacities (273.15 K, 1 bar) for the optimized material P2_3 after eight cycles C1 – C8, the sorbent was degassed under vacuum at 115 °C after each cycle.

already reported that amine solutions are less stable and undergo degradation, which is not the case of solid sorbents, which are durable over several cycles (proven also for our material).

4. Conclusions

Stable hierarchically porous nitrogen-rich sorbents were prepared using cheap precursors, through a simple approach for application in post-combustion CO_2 capture. The synthetic approach using PS NPs building blocks resulted in superior textural properties and CO_2 capture capacity compared to the materials prepared without PS NPs. The presented method, though simple, is suitable for preparation of 3-D hierarchically porous materials with high porosities, specific surface areas and pore volumes. The optimized material achieved very high CO_2 capacity (9.14 mmol g^{-1}) at 273.15 K and 1 bar, which is among the highest reported for carbon-based sorbents in the literature. It is evident that this high CO_2 capture capacity was mainly due to the hierarchical pore structure, which enhanced the diffusion of CO_2 into the inner micropores. By analyzing the CO_2 capture capacity of the different materials with varying textural properties and nitrogen contents, we conclude that the CO_2 capture capacity at low pressure is primarily controlled by the presence of micropores with diameter smaller than 0.7 nm. Nevertheless, in designing materials for practical applications, it is important to tune both the pore structure (pore size distribution) and surface chemistry (nitrogen functionalities) simultaneously to combine their advantages. These materials are promising CO_2 sorbents and we believe the described approach will serve as a guide to the development of new polymer-based carbons for CO_2 capture. Because industrial sorbents are required to withstand multiple adsorption/desorption cycles, future work will focus on evaluating the stability of these sorbents under various industrial conditions.

Acknowledgments

This work was supported by a Czech Science Foundation (GACR) grant [16-22997S]. Financial support from specific university research grants [MSMT No. 20/2017] and [MSMT No 21-SVV/2018] are gratefully acknowledged. The authors are also grateful to Prof. Dr. Giuseppe Storti from ETH Zurich for helpful discussions.

Appendix A. Supplementary data

Supplementary data to this article can be found online at https://doi.org/10.1016/j.cej.2018.10.133.

References

[1] B. Dutcher, M. Fan, A.G. Russell, Amine-based CO_2 capture technology development from the beginning of 2013-a review, ACS Appl. Mater. Interfaces 7 (2015) 2137–2148.
[2] J.D. Figueroa, T. Fout, S. Plasynski, H. McIlvried, R.D. Srivastava, Advances in CO_2 capture technology-the U.S. department of energy's carbon sequestration program, Int. J. Greenhouse Gas Control 2 (2008) 9–20.
[3] M. Songolzadeh, M. Soleimani, M. Takht Ravanchi, R. Songolzadeh, Carbon dioxide separation from flue gases: a technological review emphasizing reduction in greenhouse gas emissions, Sci. World J. 828131 (2014) 1–34.
[4] Y. Li, Z.-Y. Fu, B.-L. Su, Hierarchically structured porous materials for energy conversion and storage, Adv. Funct. Mater. 22 (2012) 4634–4667.
[5] J.A. Martens, A. Bogaerts, N. De Kimpe, P.A. Jacobs, G.B. Marin, K. Rabaey, M. Saeys, S. Verhelst, The chemical route to a carbon dioxide neutral world, ChemSusChem 10 (2017) 1039–1055.
[6] A.L. Yaumi, M.Z.A. Bakar, B.H. Hameed, Recent advances in functionalized composite solid materials for carbon dioxide capture, Energy 124 (2017) 461–480.
[7] H.A. Patel, J. Byun, C.T. Yavuz, Carbon dioxide capture adsorbents: chemistry and Methods, ChemSusChem 10 (2017) 1303–1317.
[8] L. Liu, Q.-F. Deng, X.-X. Hou, Z.-Y. Yuan, User-friendly synthesis of nitrogen-containing polymer and microporous carbon spheres for efficient CO_2 capture, J. Mater. Chem. 22 (2012) 15540–15548.
[9] Z. Liu, Z. Du, H. Song, C. Wang, F. Subhan, W. Xing, Z. Yan, The fabrication of porous N-doped carbon from widely available urea formaldehyde resin for carbon dioxide adsorption, J. Colloid Interface Sci. 416 (2014) 124–132.
[10] W. Shen, W. Fan, Nitrogen-containing porous carbons: synthesis and application, J. Mater. Chem. A 1 (2013) 999–1013.
[11] D. Lee, C. Zhang, C. Wei, B.L. Ashfeld, H. Gao, Hierarchically porous materials via assembly of nitrogen-rich polymer nanoparticles for efficient and selective CO_2 capture, J. Mater. Chem. A 1 (2013) 14862–14867.
[12] C. Pevida, M.G. Plaza, B. Arias, J. Fermoso, F. Rubiera, J.J. Pis, Surface modification of activated carbons for CO_2 capture, Appl. Surf. Sci. 254 (2008) 7165–7172.
[13] J. He, J.W.F. To, P.C. Psarras, H. Yan, T. Atkinson, R.T. Holmes, D. Nordlund, Z. Bao, J. Wilcox, Tunable polyaniline-based porous carbon with ultrahigh surface area for CO_2 capture at elevated pressure, Adv. Energy Mater. 6 (1502491) (2016) 1–11.
[14] D. Guo, R. Shibuya, C. Akiba, S. Saji, T. Kondo, J. Nakamura, Active sites of nitrogen-doped carbon materials for oxygen reduction reaction clarified using model catalysts, Science 351 (2016) 361–365.
[15] G.P. Hao, W.C. Li, D. Qian, A.H. Lu, Rapid synthesis of nitrogen-doped porous carbon monolith for CO_2 capture, Adv. Mater. 22 (2010) 853–857.
[16] Y. Xia, R. Mokaya, G.S. Walker, Y. Zhu, Superior CO_2 adsorption capacity on n-doped, high-surface-area, microporous carbons templated from zeolite, Adv. Energy Mater. 1 (2011) 678–683.
[17] J. Wang, Y. Lin, Q. Yue, K. Tao, C. Kong, L. Chen, N-rich porous carbon with high CO_2 capture capacity derived from polyamine-incorporated metal–organic framework materials, RSC Adv. 6 (2016) 53017–53024.
[18] X. Zhu, S. Chai, C. Tian, P.F. Fulvio, K.S. Han, E.W. Hagaman, G.M. Veith, S.M. Mahurin, S. Brown, H. Liu, S. Dai, Synthesis of porous, nitrogen-doped adsorption/diffusion carbonaceous membranes for efficient CO_2 separation, Macromol. Rapid Commun. 34 (2013) 452–459.
[19] W. Xing, C. Liu, Z. Zhou, L. Zhang, J. Zhou, S. Zhuo, Z. Yan, H. Gao, G. Wang, S.Z. Qiao, Superior CO_2 uptake of N-doped activated carbon through hydrogen-bonding interaction, Energy Environ. Sci. 5 (2012) 7323–7327.
[20] M. Peyravi, Synthesis of nitrogen doped activated carbon/polyaniline material for CO_2 adsorption, Polym. Adv. Technol. 29 (2018) 319–328.
[21] A. Sanchez-Sanchez, F. Suarez-Garcia, A. Martinez-Alonso, J.M. Tascon, Influence of porous texture and surface chemistry on the CO_2 adsorption capacity of porous carbons: acidic and basic site interactions, ACS Appl. Mater. Interfaces 6 (2014) 21237–21247.
[22] M. Sevilla, P. Valle-Vigon, A.B. Fuertes, N-doped polypyrrole-based porous carbons for CO_2 capture, Adv. Funct. Mater. 21 (2011) 2781–2788.
[23] E.V. Shlyakhova, L.G. Bulusheva, M.A. Kanygin, P.E. Plyusnin, K.A. Kovalenko, B.V. Senkovskiy, A.V. Okotrub, Synthesis of nitrogen-containing porous carbon using calcium oxide nanoparticles, Phys. Status Solidi 251 ((b) 2014,) 2607–2612.
[24] F. Liu, K. Huang, Q. Wu, S. Dai, Solvent-free self-assembly to the synthesis of nitrogen-doped ordered mesoporous polymers for highly selective capture and conversion of CO_2, Adv. Mater. 29 (1700445) (2017) 1–8.
[25] L. Zhou, J. Fan, G. Cui, X. Shang, Q. Tang, J. Wang, M. Fan, Highly efficient and reversible CO_2 adsorption by amine-grafted platelet SBA-15 with expanded pore diameters and short mesochannels, Green Chem. 16 (2014) 4009–4016.
[26] C.S. Srikanth, S.S. Chuang, Spectroscopic investigation into oxidative degradation of silica-supported amine sorbents for CO_2 capture, ChemSusChem 5 (2012) 1435–1442.
[27] D.M. D'Alessandro, B. Smit, J.R. Long, Carbon dioxide capture: prospects for new materials, Angew. Chem. Int. Ed. Engl. 49 (2010) 6058–6082.
[28] A. Beltzung, A. Klaue, C. Colombo, H. Wu, G. Storti, M. Morbidelli, Polyacrylonitrile nanoparticle-derived hierarchical structure for CO_2 capture, Energy Technol. 6 (2018) 718–727.
[29] Z. Rozlívková, M. Trchová, M. Exnerová, J. Stejskal, The carbonization of granular polyaniline to produce nitrogen-containing carbon, Synth. Met. 161 (2011) 1122–1129.
[30] M. Olivares-Marín, M.M. Maroto-Valer, Development of adsorbents for CO_2 capture from waste materials: a review, Greenhouse Gases: Sci. Technol. 2 (2012) 20–35.

[31] M. Sevilla, A.B. Fuertes, Sustainable porous carbons with a superior performance for CO_2 capture, Energy Environ. Sci. 4 (2011) 1765–1771.
[32] N.P. Wickramaratne, M. Jaroniec, Importance of small micropores in CO_2 capture by phenolic resin-based activated carbon spheres, J. Mater. Chem. A 1 (2013) 112–116.
[33] X. Li, T. Guo, L. Zhu, C. Ling, Q. Xue, W. Xing, Charge-modulated CO_2 capture of C_3N nanosheet: Insights from DFT calculations, Chem. Eng. J. 338 (2018) 92–98.
[34] X. Li, Q. Xue, D. He, L. Zhu, Y. Du, W. Xing, T. Zhang, Sulfur-Nitrogen codoped graphite slit-pore for enhancing selective carbon dioxide adsorption: insights from molecular simulations, ACS Sustainable Chem. Eng. 5 (2017) 8815–8823.
[35] X. Li, L. Zhu, Q. Xue, X. Chang, C. Ling, W. Xing, Superior selective CO_2 Adsorption of C_3N Pores: GCMC and DFT simulations, ACS Appl. Mater. Interfaces 9 (2017) 31161–31169.
[36] M. Sevilla, J.B. Parra, A.B. Fuertes, Assessment of the role of micropore size and N-doping in CO_2 capture by porous carbons, ACS Appl. Mater. Interfaces 5 (2013) 6360–6368.
[37] A.J. Rennie, P.J. Hall, Nitrogen-enriched carbon electrodes in electrochemical capacitors: investigating accessible porosity using CM-SANS, Phys. Chem. Chem. Phys. 15 (2013) 16774–16778.
[38] C. Liu, W. Xing, J. Zhou, S.-P. Zhuo, N-containing activated carbons for CO_2 capture, Int. J. Smart Nano Mater. 4 (2013) 55–61.
[39] M. Seredych, J. Jagiello, T.J. Bandosz, Complexity of CO_2 adsorption on nanoporous sulfur-doped carbons – is surface chemistry an important factor? Carbon 74 (2014) 207–217.
[40] J.H. Lee, H.J. Lee, S.Y. Lim, B.G. Kim, J.W. Choi, Combined CO_2-philicity and ordered mesoporosity for highly selective CO_2 capture at high temperatures, J. Am. Chem. Soc. 137 (2015) 7210–7216.
[41] B. Li, Y. Duan, D. Luebke, B. Morreale, Advances in CO_2 capture technology: a patent review, Appl. Energy 102 (2013) 1439–1447.
[42] E.M. Kutorglo, F. Hassouna, D. Kopecký, L. Fišer, I. Sedlářová, A. Zadražil, M. Šoóš, Synthesis of conductive macroporous composite polymeric materials using porogen-free method, Colloids Surf. A: Phys. Eng. Aspects (2017), https://doi.org/10.1016/j.colsurfa.2017.10.082.
[43] T.K. Das, S. Prusty, Review on conducting polymers and their applications, Polym. Plast. Technol. Eng. 51 (2012) 1487–1500.
[44] S. Bhadra, D. Khastgir, N.K. Singha, J.H. Lee, Progress in preparation, processing and applications of polyaniline, Prog. Polym. Sci. 34 (2009) 783–810.
[45] C. Dhand, M. Das, M. Datta, B.D. Malhotra, Recent advances in polyaniline based biosensors, Biosens. Bioelectron. 26 (2011) 2811–2821.
[46] D. Kim, Y. Tian, H.J. Choi, Seeded swelling polymerized sea urchin-like core–shell typed polystyrene/polyaniline particles and their electric stimuli-response, RSC Adv. 5 (2015) 81546–81553.
[47] S. Bousalem, S. Benabderrahmane, Y.Y.C. Sang, C. Mangeney, M.M. Chehimi, Covalent immobilization of human serum albumin onto reactive polypyrrole-coated polystyrene latex particles, J. Mater. Chem. 15 (2005) 3109–3116.
[48] C. Mangeney, M. Fertani, S. Bousalem, M. Zhicai, S. Ammar, F. Herbst, P. Beaunier, A. Elaissari, M.M. Chehimi, Magnetic Fe_2O_3-polystyrene/PPy core/shell particles: bioreactivity and self-assembly, Langmuir 23 (2007) 10940–10949.
[49] D.B. Cairns, M.A. Khan, C. Perruchot, A. Riede, S.P. Armes, Synthesis and characterization of polypyrrole-coated poly(alkyl methacrylate) latex particles, Chem. Mater. 15 (2003) 233–239.
[50] A.M. Youssef, Morphological studies of polyaniline nanocomposite based mesostructured TiO_2 nanowires as conductive packaging materials, RSC Adv. 4 (2014) 6811.
[51] F. Rouquerol, J. Rouquerol, K. Sing, Adsorption by Powders and Porous Solids. Principles, Methodology and Applications, Academic Press, London, 1999, pp. 166–168.
[52] M. Sevilla, C. Falco, M.-M. Titirici, A.B. Fuertes, High-performance CO_2 sorbents from algae, RSC Adv. 2 (2012) 12792–12797.
[53] J. Kou, L.-B. Sun, Fabrication of nitrogen-doped porous carbons for highly efficient CO_2 capture: rational choice of a polymer precursor, J. Mater. Chem. A 4 (2016) 17299–17307.
[54] L.Y. Meng, S.J. Park, Effect of heat treatment on CO_2 adsorption of KOH-activated graphite nanofibers, J. Colloid Interface Sci. 352 (2010) 498–503.
[55] A.-N.A. El-Hendawy, An insight into the KOH activation mechanism through the production of microporous activated carbon for the removal of Pb^{2+} cations, Appl. Surf. Sci. 255 (2009) 3723–3730.
[56] S. Mentus, G. Ciric-Marjanovic, M. Trchova, J. Stejskal, Conducting carbonized polyaniline nanotubes, Nanotechnology 20 (245601) (2009) 1–10.
[57] J. Wang, I. Senkovska, M. Oschatz, M.R. Lohe, L. Borchardt, A. Heerwig, Q. Liu, S. Kaskel, Imine-linked polymer-derived nitrogen-doped microporous carbons with excellent CO_2 capture properties, ACS Appl. Mater. Interfaces 5 (2013) 3160–3167.
[58] F.Q. Liu, L.L. Wang, G.H. Li, W. Li, C.Q. Li, Hierarchically structured graphene coupled microporous organic polymers for superior CO_2 capture, ACS Appl. Mater. Interfaces 9 (2017) 33997–34004.
[59] E. Zera, W. Nickel, G.P. Hao, L. Vanzetti, S. Kaskel, G.D. Sorarù, Nitrogen doped carbide derived carbon aerogels by chlorine etching of a SiCN aerogel, J. Mater. Chem. A 4 (2016) 4525–4533.
[60] A.K. Mishra, S. Ramaprabhu, Nanostructured polyaniline decorated graphene sheets for reversible CO_2 capture, J. Mater. Chem. 22 (2012) 3708–3712.
[61] M.S. Shafeeyan, W.M.A.W. Daud, A. Houshmand, A. Arami-Niya, Ammonia modification of activated carbon to enhance carbon dioxide adsorption: effect of pre-oxidation, Appl. Surf. Sci. 257 (2011) 3936–3942.
[62] A.P. Katsoulidis, M.G. Kanatzidis, Phloroglucinol based microporous polymeric organic frameworks with $-OH$ functional groups and high CO_2 capture capacity, Chem. Mater. 23 (2011) 1818–1824.
[63] M.G. Schwab, B. Fassbender, H.W. Spiess, A. Thomas, X. Feng, K. Mullen, Catalyst-free preparation of melamine-based microporous polymer networks through schiff base chemistry, J. Am. Chem. Soc. 131 (2009) 7216–7217.
[64] M.G. Plaza, F. Rubiera, J.J. Pis, C. Pevida, Ammoxidation of carbon materials for CO_2 capture, Appl. Surf. Sci. 256 (2010) 6843–6849.
[65] W. Xing, C. Liu, Z. Zhou, J. Zhou, G. Wang, S. Zhuo, Q. Xue, L. Song, Z. Yan, Oxygen-containing functional group-facilitated CO_2 capture by carbide-derived carbons, Nanoscale Res. Lett. 9 (189) (2014) 1–8.
[66] M.L. Gray, J.S. Hoffman, D.C. Hreha, D.J. Fauth, S.W. Hedges, K.J. Champagne, H.W. Pennline, Parametric study of solid amine sorbents for the capture of carbon dioxide, Energy Fuels 23 (2009) 4840–4844.